Frascati Physics Series Vol. XXX (1997), pp. 000-000
Conference Title - Conference Town, Oct 3rd, 1996

SEARCH FOR THE LEPTON FLAVOUR VIOLATING DECAY $\boldsymbol{\mu \to e\gamma}$.

Peter-Raymond Kettle,
Paul Scherrer Institut, PSI, CH-5232 Villigen-PSI, Switzerland

on Behalf of the MuEGamma Collaboration
BINP, Novosibirsk – KEK – Osaka University – University of Pisa – INFN, Pisa – PSI – University of Tokyo – Waseda University

ABSTRACT

Preparations are currently underway for an experimental search for the Lepton Flavour Violating (LFV) decay $\boldsymbol{\mu \to e\gamma}$ at a sensitivity down to 10^{-14}. The planned experiment, at the Paul Scherrer Institute (PSI) will utilize an intense surface muon beam, together with a gradient-field solenoidal spectrometer and a liquid Xenon calorimeter, to detect both the positron and photon respectively, from such a decay.

1 Introduction

The Standard Model of strong and electroweak interactions (SM) is seen as a low-energy approximation of a more fundamental theory. In the former, quantities such as baryon number, individual lepton number or lepton flavour and total lepton number are seen as symmetries and conserved: lepton flavour conservation arising from assumed vanishing neutrino masses in the Minimal Standard Model. Hence signatures such as $\mu \to e\gamma$, $\mu \to$e–conversion, $\mu \to 3e$, ${K^0}_L \to \mu e$, $Z^0 \to \mu e$, ν–oscillations or neutrinoless double-beta decay ($0\nu\beta\beta$–decay) are sensitive tools with which to probe physics beyond the SM.

With recent breakthroughs in the atmospheric– and solar–neutrino sectors [1, 2], evidence for flavour changing oscillations and hence neutrino masses has been provided as the plausible explanation for both the 'Solar Neutrino Problem', characterized by reduced, measured solar ν_e–fluxes [3, 4, 5, 6, 7] and the 'Atmospheric Anomaly', with its reduced atmospheric ν_μ–fluxes. In addition to this, there have also been reports of evidence for proton decay from a re-analysis of Kolar Gold Fields data [8] and reports of evidence for $0\nu\beta\beta$–decay from the Heidelberg-Moscow experiment [9], as well as indications of a deviation from the expectation of the measurements of the anomalous magnetic moment of the muon by the Brookhaven E821 experiment [10]

This adds further impetus to the search for LFV in the charged lepton sector. There are many candidates for a theory beyond the SM, with extensions including ordinary neutrino masses and their mixing predicting unmeasurably small LFV-rates, whereas supersymmetric (SUSY) extensions and especially grand unified theories (SUSY-GUT) turn out to be particularly favourable to LFV [11, 12] where additional sources of flavour mixing now come from sleptons, the scalar partners of the leptons. In fact, the predicted branching ratio of $\mu \to e\gamma$, in SU(5) SUSY-GUT

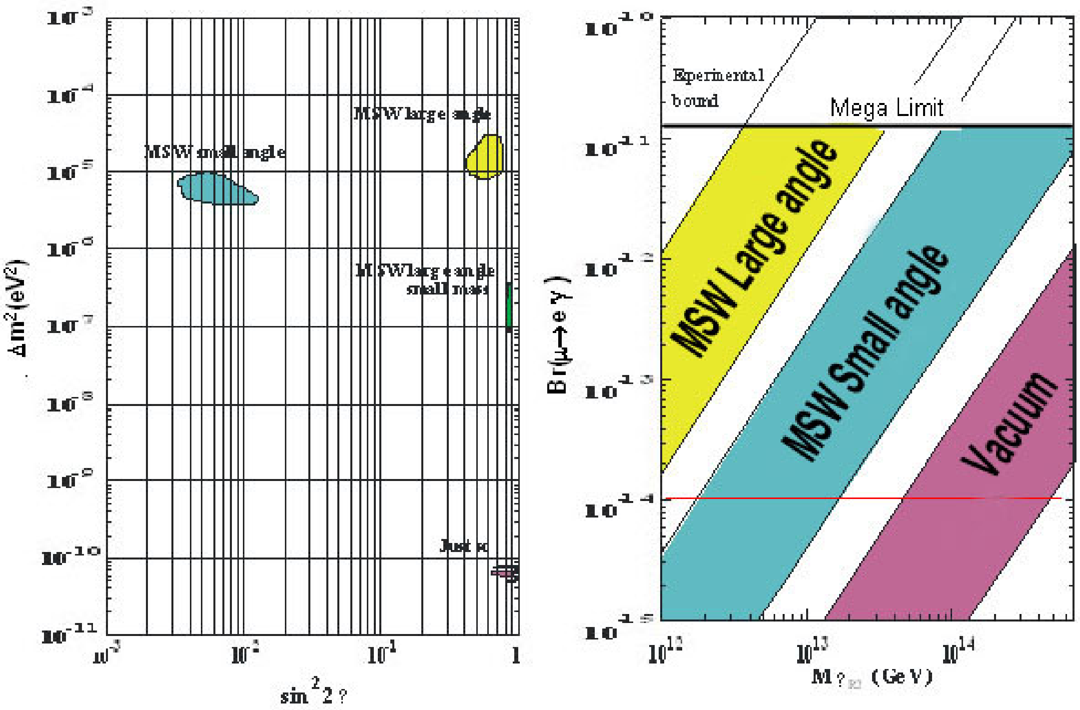

Figure 1: *$\mu \to e\gamma$ branching ratio as a function of the heavy Majorana neutrino mass as predicted by SU(5) SUSY-GUT model with right-handed neutrinos, for various solar-neutrino oscillation solutions (MSW-Large angle, MSW-Small angle and Vacuum Solution). The present MEGA-limit, as well as the proposed sensitivity of* 10^{-14} *for the new PSI-experiment, are shown.*

models range from 10^{-15} to 10^{-13} for a singlet selectron mass range between 100 – 300 GeV and even more optimistically in the case of SO(10) SUSY-GUT models where the predictions lie between 10^{-13} to 10^{-11}.

In extensions to SU(5) SUSY-GUT models, which include right-handed, Majorana neutrinos, LFV processes are expected to be enhanced with predictions, for example, of the lower bound of the branching ratios of $\mu \to e\gamma$, $\tau \to \mu\gamma$ and μ–e conversion on Ti giving 10^{-14}, 10^{-9}, and 10^{-16}, respectively [13, 14, 15]. Figure 1 shows the example for the branching ratio $\mu \to e\gamma$ in such a model [15] for various solutions to the 'Solar Neutrino Problem'. Current arguments based on a global analysis of all solar neutrino experimental data favours the MSW Large angle solution e.g. [16], thus making the prospects for a LFV-search in the charged lepton sector very attractive.

2 LFV-Searches in the muon sector

Experimental searches for LFV have a long history, going as far back as 1947, when Hincks and Pontecorvo first searched for $\mu \to e\gamma$ using cosmic rays [17]. The upper limits for such searches have steadily improved at a rate of approximately two-orders of magnitude per decade, with some of the most sensitive measurements coming from the meson factories, in the muon sector e.g. $\mu \to e\gamma$, $\mu \to$e–conversion, $\mu \to 3e$. The

Table 1: *Current LFV-Limits in the muon sector, predominantly from the meson factories, references from PDG* [18].

Reaction	Present Limit	PDG Lepton Listing Ref.
$Br(\mu^+ \to e^+\gamma)$	$< 1.2\cdot10^{-11}$	*Brooks et al.* 99 *LAMPF*
$Br(\mu^+ \to e^+2\gamma)$	$< 7.2\cdot10^{-11}$	*Bolton et al.* 88 *LAMPF*
$Br(\mu^+ \to e^+e^-e^+)$	$< 1\cdot10^{-12}$	*Bellgardt et al.* 88 *PSI*
$B(\mu^-Ti \to e^-Ti)$	$< 6.1\cdot10^{-13}$	*Wintz et al.* 98 *PSI*
$B(\mu^-Pb \to e^-Pb)$	$< 4.6\cdot10^{-11}$	*Honecker et al.* 96 *PSI*
$B(\mu^-S \to e^-S)$	$< 7\cdot10^{-11}$	*Badertscher et al.* 80 *SIN/PSI*
$B(\mu^-Cu \to e^-Cu)$	$< 1.6\cdot10^{-8}$	*Bryman et al.* 72 *SREL*
$P_{M\overline{M}}(\mu^+e^- \to \mu^-e^+)$	$< 8.3\cdot10^{-11}$	*Willmann et al.* 99 *PSI*
$B(\mu^-Ti \to e^+Ca)$	$< 3.6\cdot10^{-11}$	*Kaulard et al.* 98 *PSI*
$B(\mu^-S \to e^+Si)$	$< 9\cdot10^{-10}$	*Badertscher et al.* 80 *SIN/PSI*
$B(\mu^-Cu \to e^+Co)$	$< 2.6\cdot10^{-8}$	*Bryman et al.* 72 *SREL*

Paul Scherrer Institute PSI, with its high intensity surface muon beams also has a long tradition of LFV-searches using muons, see Table 1 for some of the most competitive limits predominatly from the meson factories.

2.1 Present Generation Experiments

2.1.1 MEGA-Experiment at LAMPF

The current best limit for the LFV-decay $\mu \rightarrow e\gamma$ comes from the MEGA-experiment [19] undertaken at the stopped muon channel at the Los Alamos Meson Physics Facility LAMPF. Over a period of 3 years, a total of $1.2 \cdot 10^{14}$ surface muons were stopped in a target, centred in a solenoidal magnetic field of 1.5 T. The beam intensity was $2.5 \cdot 10^{8}$/s, with a macroscopic duty factor of 6%. The positrons from stopped muon decay were detected in the magnetic spectrometer by using a set of eight high-rate cylindrical multi-wire proportional chambers (MWPCs) and timing scintillators. Three concentric pair-spectrometers, surrounding the positron spectrometer, were used in conjunction with drift chambers and MWPCs to determine the energy and direction of the photon. Based on the full data-set, a new upper limit on the branching ratio of $\mathrm{Br}(\mu \rightarrow e\gamma) < 1.2 \cdot 10^{-11}$ with 90% confidence was established.

2.1.2 Sindrum II at PSI

In the case of μ–e conversion, measurements undertaken by the Sindrum II collaboration at PSI, have yielded the most sensitive limits on LFV muon decays, cf. Table 1. The coherent, neutrinoless conversion of a negative muon to an electron in a muonic atom (μ–e conversion) has a very clear event signature, namely, a mono-energetic single electron, with an energy equal to the difference between the muon mass and the sum of the binding energy of the 1s- state of the muonic atom and the nuclear recoil energy: $E_{\mu e}=(M_\mu - B_\mu - E_{rec})$, giving $\sim$ 95MeV for Lead, 96 MeV for Gold and 104 MeV for Titanium. This is well above the end-point energy of the Michel spectrum from normal muon decay (52.8 MeV) and hence, together with the fact that the search is for a single particle, is a great advantage from an experimental point of view. However, backgrounds do exist, the dominant ones being, muon decay in orbit (MIO), which has the same electron end-point energy, though highly suppressed at the end-point. Radiative muon (RMC) and pion capture (RPC) involve either internal or external, asymmetric e^+e^- conversion of the photon, of which the e^+ is not seen. In the case of RPC the photon energy reaches above the end-point energy of the sought after electron, this necessitates the high suppression of any pion contamination. Finally, cosmic induced electrons can be suppressed, with good tracking capabilities. The Sindrum II collaboration, having reached an upper limit of $6.1 \cdot 10^{-13}$ for μ–e conversion on Ti, is currently analyzing data taken with a gold target, as current predictions of the conversion probability favour a linear rise with atomic weight. The detector consists of a superconducting solenoidal spectrometer, with a thin Au-target placed axially at the centre. A 52 MeV/c μ^--beam is separated from pion contamination, via a degrader, some 8.5 m upstream at the start of large transport solenoid (PMC). The lone electron signature is searched for, using a combination of scintillator and Cernekov hodoscopes, together with drift chambers. A preliminary result [20], in view of no observed signal, was recently given as: B(Au) $< 6 \cdot 10^{-13}$ at 90% C.L., relative to the capture channel.

2.2 Future Generation Experiments

The next generation experiments in the LFV muon sector are currently in the preparation or planning phase. A μ–e conversion search at Brookhaven National Laboratory BNL, proposal E940 at the BNL-AGS [21], called MECO (Muon–Electron–COnversion) is planning a single event sensitivity of $\sim 2 \cdot 10^{-17}$ for an aluminium target. In order to achieve its goal MECO will use three adiabatic superconducting solenoids, the first, to capture the muons from the proton bombarded, tungsten production target, the second, an S-shaped element, used for transporting, filtering and selecting and finally, the detector solenoid with a straw-tube tracker and crystal calorimeter.

There are also plans for a future μ–e conversion experiment, PRIME, which could be implemented at the proposed high intensity, slow muon facility PRISM, which would provide about 10^{11}–10^{12} muons/s combined with the 50 GeV PS of the joint KEK-JAERI project, which is now under construction. PRIME would aim at a sensitivity of $\sim 10^{-18}$.

Finally, a new $\mu \to e\gamma$ search is in preparation at PSI [22] planning a sensitivity down to the 10^{-14} level. This experiment will be described in more detail in the following sections.

3 PSI MuEGamma Experiment

3.1 Overview

The experiment aims to search for the LFV decay $\mu \to e\gamma$ with a sensitivity down to 10^{-14}. To achieve this, both a high intensity source of stopped muons and detectors capable of resolving the positron and photon from the decay, with high efficiency and good energy, timing and positional resolutions are required, as well as novel features. A schematic view of the detector is shown in Figure 2. Surface muons

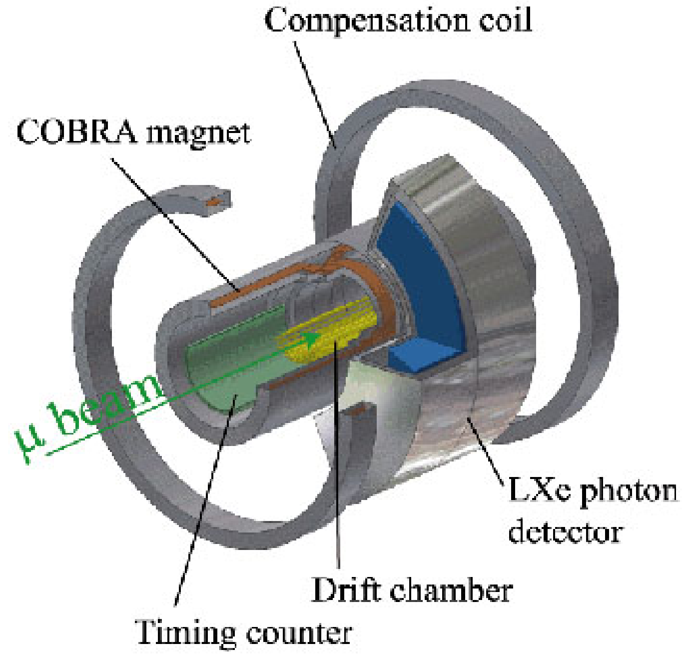

Figure 2: *Schematic view of the proposed detector for the PSI $\mu \rightarrow e\gamma$ experiment, showing the main features: COBRA positron spectrometer consisting of the superconducting gradient field solenoid, tracking drift chambers, and timing counters. The photon detection side consists of a 'mini-Kamiokonde' type, large volume LXe calorimeter with compensation coils to reduce the stray B-field at the calorimeter photomultipliers.*

at an initial momentum of 28 MeV/c enter the thin-coil, superconducting solenoid and are stopped in a small, thin target. The subsequent decay of the muon leads to a positron, which exhibits a spiral path with increasing pitch, the bending radius of which depends entirely on its total momentum and is 'independent' of its emission angle. These novel features are achieved by use of the gradient field of the solenoid magnet, with a maximum field strength of 1.27 T at the centre of the detector, decreasing axially. The positron momentum and angle are determined by tracking the particle with a set of azimuthally spaced, staggered-cell drift chambers, while the energy, timing and angle of the photon are obtained from a liquid Xenon calorimeter, viewed from all sides by some 800 photomultiplier tubes. The timing of the positron and hence the trigger condition for coincident, back-to-back decay products, is given by a set of fast, double-layered, orthogonally placed, scintillator timing-counter arrays, positioned at opposite ends of the detector.

3.2 Signal Sensitivity & Backgrounds

The signature for a $\mu \rightarrow e\gamma$ event is kinematically simple, one expects a back-to-back positron and photon of a well defined energy (52.8 MeV) coincident in time. One of the main sources of background comes from so-called 'prompt events' or radiative muon decays $\mu^+ \rightarrow e^+\nu_e\overline{\nu}_\mu\gamma$ in which little energy is carried away by the neutrinos and the e^+ and γ go back-to-back. Another source of background, which becomes increasingly important as the beam intensity increases, is 'accidental' overlapping of events in which e.g. the Michel e^+ from one muon decay is detected in coincidence with a back-to-back photon of the correct energy, coming from e.g. the annihilation-in-flight of a Michel e^+ from another muon decay.

The expected single-event-sensitivity for a running time T of $\sim$ 50 weeks is shown in eq.1, for a planned muon stopping-rate of $1{\cdot}10^8$/sec and a solid angle coverage $\Omega/4\pi$ of $\sim$9%. The positron and photon detection efficiencies were taken as ϵ_e= 0.95 and ϵ_γ = 0.7 respectively as well as an event selection efficiency of ϵ_{sel} = 0.8.

$$Br(\mu \rightarrow e\gamma) = (N_\mu \cdot T \cdot \Omega/4\pi \cdot \epsilon_e \cdot \epsilon_\gamma \cdot \epsilon_{sel})^{-1} = 0.94 \cdot 10^{-14} \tag{1}$$

The corresponding level of the 'prompt', radiative background is expected to be at a level $< 10^{-16}$, whereas the effective branching ratio for the 'accidental' background, which is described by the expression in eq. 2, corresponds to $\sim 5{\cdot}10^{-15}$ for

$$B_{acc} \propto \Delta E_e \cdot \Delta t_{e\gamma} \cdot (\Delta E_\gamma)^2 \cdot (\Delta\theta_{e\gamma})^2 \tag{2}$$

the expected individual energy–(ΔE_e, ΔE_γ) and combined timing-($\Delta t_{e\gamma}$) and angular–resolutions ($\Delta\theta_{e\gamma}$) of the positron and photon.

3.3 Positron Detection

Positron detection is achieved using the 'COnstant Bending RAdius' spectrometer COBRA, comprised of a five-coil, thin superconducting solenoid, with three radii, in order to obtain a gradient magnetic field, decreasing from (1.3–0.5) T from the centre out, axially. The material thickness of the coils and cryostat amounts to $\sim$3 g/cm^2, corresponding to a transmission coefficient of 95% for 52.8 MeV photons. A set of double-planed, staggered-cell, radially-aligned drift chambers are envisaged for the positron tracking, while for precise timing and trigger information, a set of double-layered, orthogonally placed, scintillator hodoscopes will be used. A view of the main features of the detector are shown in Figure 3.

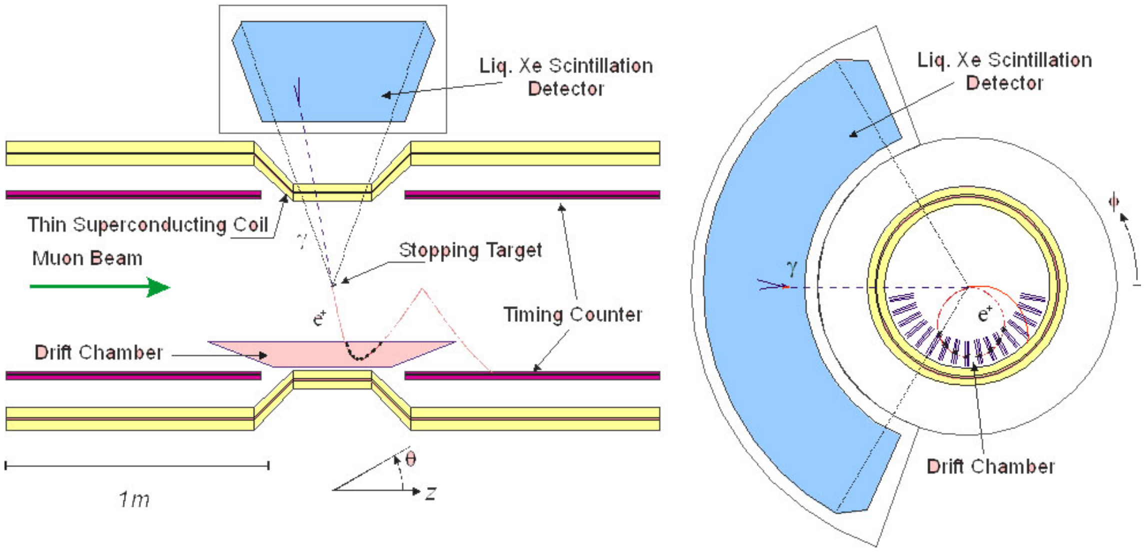

Figure 3: *Cross-sectional view of the PSI MuEGamma detector, showing the plan view (l.h.s) and side-elevation view (r.h.s) along with the main features of the COBRA positron spectrometer in addition the LXe calorimeter is shown.*

3.3.1 Gradient Field Concept

The advantages of using a gradient field are two-fold: firstly, unlike the situation in a constant solenoidal magnetic field, where the bending radius of a charged particle is proportional to the transverse momentum component P_T and hence dependent on the emission angle, monochromatic particles are caused not only to have different radii depending on the angle, but also those particles with large emission angles are caused to 'curl-up' resulting in many hits in the chambers. In the case of a gradient field, these two disadvantages can be overcome, as shown in Figure 4, where the bending radius is shown to be proportional to the total momentum, independent of emission angle and those particles with large emission angles are swept-out of the detector with fewer hits. This also allows particles of a given momentum to be selected, according to their radii in the chambers.

3.3.2 Positron Tracking Devices

The tracking devices will consist of a set of 16 planar, open-framed drift chambers, located axially at the centre of the detector and will be radially aligned at 10° intervals azimuthally. Each chamber consists of a double-layer with a staggered cell structure between adjacent layers. Each layer will also consist of vernier patterned

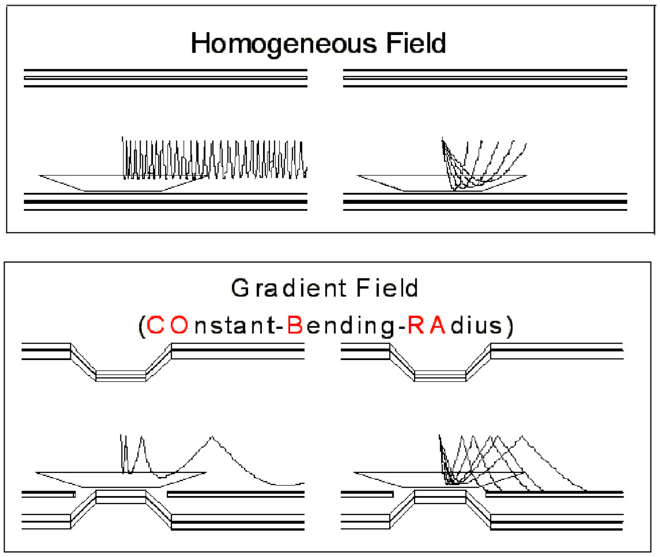

Figure 4: *Schematic view showing the principle of the COBRA spectrometer. The gradient magnetic field gives a constant bending radius for a monochromatic particle, independent of emission angle (see r.h.s). Particles emitted close to 90° are swept out of the sensitive tracking region faster and with fewer hits than in the case of a homogeneous field.*

cathode strips, from which the charge information will be used to determine the axial coordinate. The radial coordinate of a hit is given by the difference in signal arrival times of adjacent layered cells, whereas the absolute time is given by the mean time of the same two signals. The axial coordinate of the hit will be determined initially, with a coarser resolution, from the charge information of the hit wire, using the charge-division method. Following which, by using the charge ratios from the vernier strips of each layer a resolution of 300 microns axially is expected, whereas $\sim$ 200 microns is expected radially. A helium based gas mixture will be used in order to reduce multiple scattering. The expected reconstructed momentum resolution for positrons is 0.7% (FWHM).

3.3.3 Positron Timing Counters

In order to suppress background events caused by an overlapping signature of mutiple muon decays, good timing resolution is necessary in order to well-define the coincidence between a candidate photon and positron. Since the timing resolution from the drift chambers is of the order of 5ns, while that of the photon calorimeter is expected to be at the 100 ps level, a better match is needed on the positron side. To facilitate this, a set of fast, double-layered, orthogonally aligned, scintillator timing-counter arrays, positioned at opposite ends of the detector, will be used.

The active axial length of the timing counters will cover $\sim$ 1m and the azimuthal coverage will be about 120°. Positrons of 52.8 MeV emitted within a polar angle between $70° <| \theta |<85°$ will produce a hit on the timing counters after approximately 1.5 turns. Both layers of scintillators will be read out from either end, giving both timing and pulse-height information, this will yield the impact point of the positron by two independent methods. Firstly, as the scintillator edges have a slanted overlap, it is expected that two or three scintillator staves will be hit, the pulse-height ratios of which will yield the impact point to within about ± 1 cm axially and ± 3 cm in ϕ. Secondly, from the timing differences of each counter the impact point will be provided, hence the correlation to a coincident photon, is given with similar accuracy to that of the calorimeter.

3.4 Photon Detection

To meet the stringent requirements of excellent energy, timing and spatial resolutions the photon detection side of the experiment is based on homogeneous response and spatial non-segmentation. The use of a liquid Xenon (LXe) calorimeter, containing some 800 l of liquid ($\sim 2.4t$) at -100°C is planned. Compared to organic scintillator crystals, the high light yield, $\sim$75% of NaI(Tl) and fast response time (45 ns decay time) as well as the homogenaity should outweigh the technical complexity of maintaining such a large volume of cryogenic noble gas. The design of the final vessel is shown in Figure 5. In the mini 'Kamiokande'-type of calorimeter the Xe fiducial volume, having a radial depth of 47 cm, will be viewed from all sides by 800 Photomultiplier tubes (PMTs), immersed in the liquid at -100°C, giving a solid angle coverage of about 12%. The expected reconstructed shower-foot resolutions in the lateral and longitudinal directions are 4mm and 16 mm (FWHM) respectively, with an energy resolution of $\sim$2% and an overall timing resolution of 100ps expected.

Owing to the technical complexity of such a device, the final design can only be realized by studying the characteristics of various, realistic prototypes. So far, two prototypes have been built, the so-called 'small' prototype, with 2.3 l of LXe viewed in total by 32 PMTs, used to test the principle as well as the technical difficulties of operating PMTs in a liquid, at this temperature. Radioactive source studies were also undertaken, to measure the energy, position and timing resolutions. The results agree consistently with simulations, as do the values obtained by scaling from the source energies to 52.8 MeV, however, the extrapolation from 2 MeV to

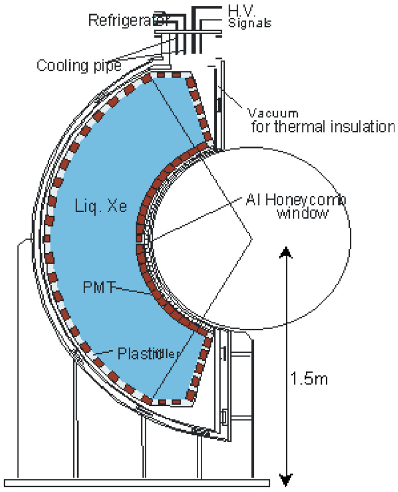

Figure 5: *Cross-sectional view of the Liquid Xenon photon calorimeter, as viewed in the beam direction. The 800l of liquid Xe making up the mini'Kamiokande'-type of detector will be viewed from all sides by 800 PMTs, immersed in the liquid at -100°.*

52.8 MeV should be taken with caution and can only be confirmed by means of measurements taken with photons of that energy.

A 'large' prototype detector has also been constructed recently and is currently under test. This contains 150 l of LXe viewed by 264 PMTs and will be used to measure the above-mentioned resolutions at an energy close to that of 52.8 MeV, by using the 40 MeV photons produced at the Compton backscatter facility, by the TERAS storage ring at ETL, Tsukuba in Japan.

4 Conclusion

There is a strong physics motivation in the search for LFV, especially in the muon sector. Recent results have shown that extensions to the SM are necessary, however, it is up to future experiments to determine which form is correct. If predictions concerning SUSY and SUSY-GUTs turn out to be correct then there are very favourable conditions for future experiments using high intensity muon sources, such as MECO at BNL and MuEGamma at PSI.

References

1. Y. Fukuda *et al.*, Phys. Rev. Lett. **81**, 1562 (1998).

2. Q.R. Ahmed *et al.*, Phys. Rev. Lett. **87**, 71301 (2001).

3. Y. Fukuda *et al.*, Phys. Rev. Lett. **77**, 1683 (1996).

4. E. Bellotti, Nucl. Phys. B (Proc. Suppl.) **91**, 44 (2001);
W. Hampel *et al.*, Phys. Lett. B **388**, 364 (1996);
P. Anselmann *et al.*, Phys. Lett. B **342**, 440 (1995).

5. V. Gavrin, Nucl. Phys. B (Proc. Suppl.) **91**, 36 (2001);
J.N. Abdurashitov *et al.*, Phys. Lett. B **328**, 234 (1994).

6. S. Fukuda *et al.*, Phys. Rev. Lett. **86**, 5651 (2001).

7. B.T. Cleveland *et al.*, Astrophys. J. **496**, 505 (1998).

8. H. Adarkar *et al.*, hep-ex/0008074 (2000).

9. H.V. Klapdor-Kleingrothaus *et al.*, Mod. Phys. Lett. A vol.16**37**, 2409 (2001).

10. H.N. Brown *et al.*, Phys. Rev. Lett. **86**, 2227 (2001).

11. R. Barbieri and L.J. Hall, Phys. Lett. B **338**, 212 (1994).

12. R. Barbieri, L.J. Hall and A. Strumia, Nucl. Phys. B **445**, 219 (1995).

13. J. Hisano *et al.*, Phys. Lett. B**357**, 576 (1995).

14. J. Hisano *et al.*, Phys. Lett. B**437**, 351 (1998).

15. J. Hisano, D. Nomura, Phys. Rev. D**59**, 116005 (1999).

16. M.B. Smy, hep-ex/0202020 (2002).
also e.g. G. Fogli, contribution to this Workshop.

17. E.P. Hincks and B. Pontecorvo, Phys. Rev. **73**, 257 (1947).

18. D.E. Groom *et al.*, Eur. Phys. J. C **15**, 1 (2000).
For Winz *et al.* see 1st Int. Symp. on Lepton & Baryon Number Violation 534 (1998).

19. M.L. Brooks *et al*, Phys. Rev. Lett. **83**, 1521 (1999);
hep-ex/0111030 (2001).

20. W. Bertl *et al.*, Proceedings hep2001 Int. Europhysics Conf. on HEP, 12th-18th July 2001, Budapest Hungary.

21. M. Backman *et al.*, BNL-AGS Proposal E940, (1997).

22. L.M. Barkov *et al.*, PSI Research Proposal R-99-05.1 (1999).